Science of Sintering, **54** (2022) 235-248

https://doi.org/10.2298/SOS2202235V

UDK: 622.785; 546.824

TiO_2 Nanotubes Film/FTO Glass Interface: Thermal Treatment Effects

Jelena Vujančević[1*)], Andjelika Bjelajac[2], Katerina Veltruska[3], Vladimir Matolin[3], Zdravko Siketić[4], Georgios Provatas[4], Milko Jakšić[4], George E. Stan[5], Gabriel Socol[6], Ion N. Mihailescu[6], Vladimir B. Pavlović[7], Djordje Janaćković[8]

[1]Institute of Technical Sciences of SASA, Knez Mihailova 35/IV, 11000 Belgrade, Serbia
[2]University of Belgrade, Innovation Center of Faculty of Technology and Metallurgy, Karnegijeva 4, 11120 Belgrade, Serbia
[3]Charles University, Faculty of Mathematics and Physics, Department of Surface and Plasma Science, V Holešovičkách 2, 180 00 Prague 8, Czech Republic
[4]Ruđer Bošković Institute, Bijenička cesta 54, 10000 Zagreb, Croatia
[5]National Institute of Materials Physics, Laboratory of Multifunctional Materials and Structures, RO-077125 Magurele, Ilfov, Romania
[6]National Institute for Lasers, Plasma, and Radiation Physics, Lasers Department, "Laser-Surface-Plasma Interactions" Laboratory, RO-077125 Magurele, Ilfov, Romania
[7]University of Belgrade, Faculty of Agriculture, Nemanjina 6, 11080 Beograd, Serbia
[8]University of Belgrade, Faculty of Technology and Metallurgy, Karnegijeva 4, 11120 Belgrade, Serbia

Abstract:

Pure Ti films deposited by radio-frequency magnetron sputtering on FTO glass were anodized to fabricate TiO_2 nanotubes (NTs) arrays. The TiO_2 NTs/FTO samples were sintered at 450, 550 and 630^oC, in ambient air. The thermal treatment did not influence the crystal phase composition, preserving in all cases the anatase single phase. As expected, the crystalline anatase quality improved with the annealing temperature. Nevertheless, slight differences in nanotubular morphology, such as the appearance of grains inside the walls, were observed in the case of the sample sintered at 630^oC.

Chemical analysis by X-ray Photoelectron Spectroscopy of annealed samples revealed the presence of Sn inside TiO_2 NTs, due to diffusion of Sn from the substrate to TiO_2. For the substrate was used FTO glass whose top layer consists of SnO_2 doped with F. Rutherford Backscattering Spectrometry and Time-of-Flight Elastic Recoil Detection Analysis were carried out to study the elemental depth profile of the films. It was found that the temperature of sintering controls the Sn diffusion inside TiO_2 film. Sn atoms diffuse towards the TiO_2 NTs surface for the samples annealed at 450 and 550^oC. The diffusion is however hindered in the case of the heat treatment at 630^oC. Besides, the Ti diffusion into the SnO_2 underlayer was observed, together with the formation of TiO_2/SnO_2 interfaces. One then expected but not a great difference in absorption between samples, since all contained anatase phase, as confirmed by Diffuse Reflectance Spectroscopy. A higher amount of Sn was

*) **Corresponding author:** jelena.vujancevic@itn.sanu.ac.rs

however detected for the sample annealed at 550°C, which accounts for a slight red absorption shift. The importance of controlling the annealing parameters of the anodized TiO_2/FTO structures was highlighted through the formation of TiO_2-SnO_2 interfaces and the Sn insertion from FTO, which can play an essential role in increasing the photoperformances of TiO_2 NTs/FTO based structures of photovoltaic cells.
***Keywords**: Sn diffusion; Sn-TiO_2 doping; Sintering; ToF-ERDA; XPS.*

1. Introduction

The conversion of solar to electrical energy via photovoltaics (PV) is a demonstrated direction aiming to solve both the world energy crisis and global warming. Production of energy using PV devices, like solar cells, is much less harmful to the environment than widely used fossil fuels. Consequently, the design of performant PV devices became an interesting research challenge and many different types of solar cells were developed, from silicon crystals [1] to organic [2], quantum dots (QD) [3,4], dye-sensitized (DSSC) [5] and the inorganic-organic perovskite solar cells [6]. Among them, DSSC, QD and perovskite solar cells are low cost and simple to fabricate. They include a sensitizer (dye, quantum dot or perovskite), a photoanode and a hole transport material or electrolyte. As a rule, the photoanode is a titanium oxide (TiO_2) based film deposited on a transparent substrate. TiO_2 is an *n*-type semiconductor that has many different applications: in solar cells [7], gas sensors [8], lithium batteries [9], for photocatalysis [10], improving mechanical performance of ceramics [11] and etc. The most used form of TiO_2 is of nanoparticles, but the drawback of this morphology is the randomization of the particle network with agglomeration and interholes. This leads to electron-hole recombination increase and loss of energy efficiency [12]. On the other hand, nanotubular morphology provides a unidirectional pathway for electron transport which reduces electron-hole recombination, increases electron diffusion length and provides a large internal surface area [13]. Different techniques were designed to synthesize nanotubular objects, such as hydrothermal [14], template [15] and anodization of titanium (Ti) foil or Ti film [16]. Among these methods, anodization of Ti foil is adequate for obtaining highly ordered and vertically aligned nanotubes on the substrate. Ti foil is an opaque material that hinders applications in solar cells due to the back-side illumination. To overcome this drawback, synthesizing transparent TiO_2 nanotubes (NTs) by anodization of Ti film deposited on a transparent substrate can be a solution. As-anodized TiO_2 NTs are amorphous, and in order to obtain a crystal structure that has much better electrical conductivity, the TiO_2 photoanode should be annealed above 400°C [17]. Due to the high-temperature annealing, different morphology and crystallinity of the NT film could be obtained. The high temperature treatment has also an impact on the transparent substrate. Usually, transparent conductive oxide (TCO) glasses are used. This type of substrate consists of sodium-lime glass covered with a thin conductive layer on the top. The conductive layer is commonly a SnO_2 (tin oxide, TO) that can be doped with fluoride (known as FTO glass) or with indium (known as ITO glass). Both FTO and ITO are commercially available, but FTO is more commonly used [18]. Although ITO has better conductivity, it is thermally unstable and less resistant to chemicals. At temperatures in excess of 350°C [19], the conductivity of ITO decreases, while FTO glass preserves conductivity stability up to 800°C (if short annealing times are applied). However, diffusion of Sn from SnO_2 layer into TiO_2 layer during thermal treatment (TT) was detected. Shinde *et al.* [20], sintered iron-coated FTO at 800°C just for a short time in order to preserve the optimum conductivity of FTO. They got Sn diffusion into α-Fe_2O_3 photoanode which enhanced the photoactivity of the photoanode. Andrei *et al.* [21] also investigated the effect of annealing temperature on a DSSC and observed the SnO_2 migration into TiO_2. Shang *et al.* [22] noticed an improved photocatalytic activity of TiO_2/SnO_2 bilayered structure due to the better charge separation. Our previous

studies [23] showed that Sn diffusion from FTO into TiO_2 nanotube arrays at 500°C had a positive impact on the photocatalytic degradation of methyl blue dye. Li *at al.* [24] also observed improved perovskite solar conversion efficiency for TiO_2 modified with SnO_2-Sb_2O_3, while Chua *et al.* [25] pointing that TiO_2 doped with Sn improved photocatalytic degradation of stearic acid due to reduction electron-hole recombination rate.

Even though these studies suggest the beneficial role of Sn diffusion in the TiO_2 active layer, herein we focus on tracking the changes that occur due to the annealing within the 450-630°C temperature range, with a special focus on the interface between TiO_2 NTs film and FTO glass. Complex information about the chemical composition of TiO_2 films was provided by X-ray Photoelectron Spectroscopy (XPS). To thoroughly characterize the TiO_2/FTO interface, a Rutherford Backscattering Spectrometry (RBS) was used for the chemical composition analysis of TiO_2 films, whereas elemental depth profiles of the films were determined via Time-of-Flight Elastic Recoil Detection Analysis (ToF-ERDA).

2. Materials and Experimental Procedures

2.1 Preparation of samples

Radio-frequency magnetron sputtering (RF-MS) was used to deposit pure Ti film onto FTO glass substrate (PI-KEM Ltd, 200 nm FTO film, 12-14 Ω cm^{-2}). Before sputtering, FTO glasses were ultrasonically cleaned in acetone and ethanol for 10 min each. After drying, the glass substrates were fixed inside a deposition chamber and a shadow mask was interposed to obtain coated areas with sizes of 10 × 10 mm^2. The sputtering was conducted at room temperature using Cesar RF Power Generator equipped with a Dressler RMC-1 Matching Controller (13.56 MHz). Pure Ti disk (Alfa Aesar GmbH) was used as a magnetron cathode target. A target-to-substrate separation distance of 40 mm was set. The FTO glass was first etched in argon plasma for 10 min and then the Ti film was deposited at a working argon gas pressure of 0.5 Pa for 60 min.

The Ti films on FTO glass were anodized under 60 V in an organic electrolyte. The electrolyte consisted of 0.3 wt.% NH_4F and 2 wt.% de-ionized water in ethylene glycol [26,27]. A platinum foil was used as a cathode and, placed 20 mm from the anode (Ti). The anodization was stopped when the film became transparent, meaning that all Ti was reacted. The samples were rinsed with water and dried naturally in the air. Then, the annealing was carried out in ambient air at three different temperatures: 450, 550 and 630°C, for 30 min, with heating speed 5 °C/min. The samples were not annealed at 650°C because the substrates started to deform at that temperature. Samples were labeled as TiO_2-450, TiO_2-550 and TiO_2-630 according to the temperature of annealing.

2.2 Characterization

The sample morphology was examined by Field Emission Scanning Electron Microscopy (FESEM), with Tescan MIRA3 XMU equipment, under 20 keV.

The crystal structure of the samples was analyzed by Grazing Incidence X-Ray Diffraction (GIXRD) using a Rigaku SmartLab 3 kW system with CuK_α radiation (λ=1.5418 Å), operating at 40 kV and 40 mA at the room temperature. The incidence angle was set at 0.25° (to maximize the signal originating from the TiO_2 NTs), and the scattered intensity was scanned within the 2θ range of 20–50° with a step size of 0.04°, and a scan speed of 0.25 degrees/min (dwell time of 9.6 s).

The X-ray Photoelectron Spectroscopy (XPS) analyses were performed using 1253.6 eV Mg K_α X-ray source to investigate the overall chemical composition of the samples. The XPS spectra were analyzed via fitting the Shirley-type function (*i.e.*, non-linear

background) and a sum of Voigt functions, using KolXPD software. The charging of spectra was corrected according to the binding energy of the adventitious carbon (284.8 eV).

Rutherford Backscattering Spectrometry is a widely used non-destructive technique, suitable for the analysis of heavier elements in a matrix of light elements, within a depth of several μm. Moreover, RBS can provide results with a nm-depth resolution and thereby, was employed to obtain the depth profiles of Ti and Sn. The measurements were carried out using a 4 MeV $^{7}Li^{3+}$ beam and the scattered ions were detected by a Silicon Surface Barrier detector placed at 165° with respect to the beam axis. The analysis of the acquired spectra was performed using SIMNRA code [28].

The elemental depth profile of the films was determined using Time-of-Flight Elastic Recoil Detection Analysis. The measurements were performed using a 23 MeV $^{127}I^{6+}$ beam, under 20° incidence angle against the sample surface, and ToF-ERDA spectrometer positioned at 37.5° with respect to the beam direction. More details about the ToF-ERDA spectrometer (and analytical method) are available in the Refs. [22,23]. Data analysis has been carried out using the simulation code Potku [31].

Diffuse Reflectance Spectroscopy (DRS) data were recorded using a Shimadzu UV-2600 spectrophotometer.

3. Results and Discussion

The surface morphology of the sputtered Ti film on the FTO glass (before anodization) is visible from Fig. 1a.

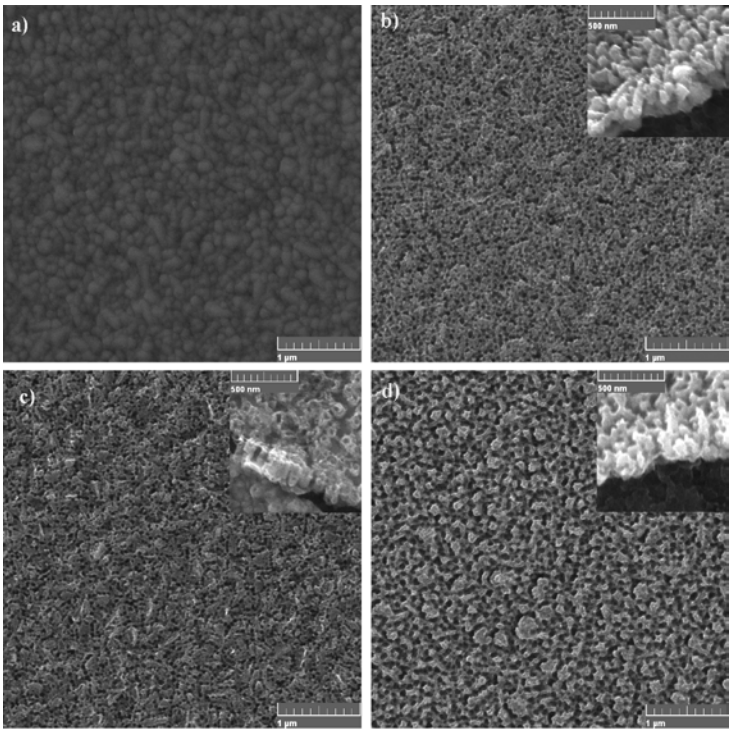

Fig. 1. Top-view FESEM micrographs of the sputtered Ti film on FTO glass (a), and TiO_2 nanotubes annealed in air at 450°C (b), 550°C (c) and 630°C (d). The cross-sectional FESEM images of the TiO_2-450, TiO_2-550 and TiO_2-630 samples are given in the corresponding insets.

The as-sputtered Ti film was dense and consisted of small tightly-packed grains with sizes ~200 nm. After anodization, the morphology of samples (Fig. 1b-d) became porous. Self-ordered ~250 nm long nanotubes were forming, with an average inner diameter of ~40 nm. The samples annealed at 450 and 550°C had a similar morphology, suggesting that up to 550°C no morphological changes are actually induced. However, at higher annealing temperature of 630°C, the nanotubular structure started to crumble. Porosity is still present, but the NT wall is now thinner and formation of grains on walls was observed (Fig. 1d).

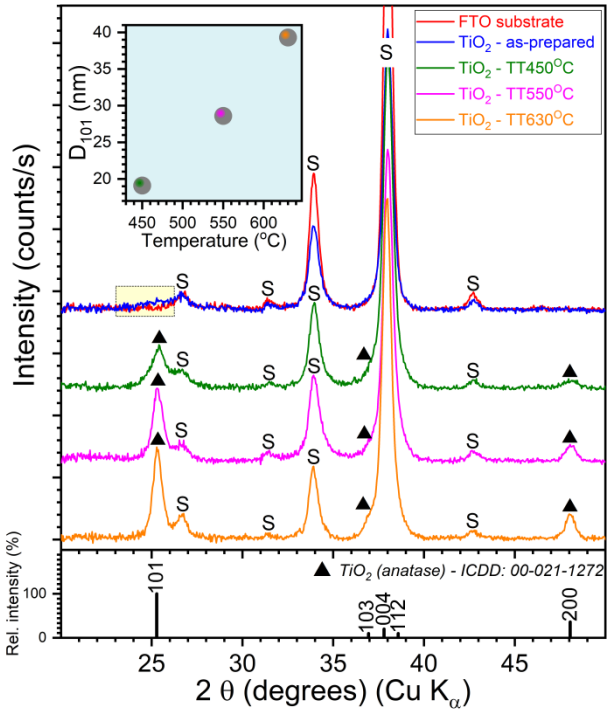

Fig. 2. GIXRD patterns of the FTO-glass substrate, bare and coated with TiO_2 nanotubes arrays (as-prepared or thermal-treated (TT) at 450, 550 and 630 °C in air for 30 min). The ICDD-PDF4+ 2018 reference file of TiO_2-anatase (no. 00-021-1272) is visible in the bottom graph for comparison. Inset: Evolution of the average crystallite size, estimated for the 101 anatase reflection, with the annealing temperature.

The GIXRD investigations, shown comparatively in Fig. 2, indicated the incremental increase of the crystalline quality of TiO_2 nanotubes array with the annealing temperature. In the case of the as-prepared TiO_2 sample, the definite diffraction maxima appertain to the substrate (a SnO_2-like phase, *e.g.*, ICDD: 00-041-1445). The absence of other peaks and the presence of a slender hump, extending from 23 to 26° in 2θ range, suggest an amorphous status (within the sensitivity limit of the XRD machine) of the as-prepared TiO_2 samples. The 101 and 200 reflections of an anatase-like TiO_2 phase (ICDD: 00-021-1272) were observed after the TT at 450°C. The increase of the annealing temperature induced an augmentation of the anatase peaks intensity, accompanied by the decrease of the full width at half maximum (FWHM), indicative of a continuous improvement of the crystalline status. The 103 anatase diffraction maxima could only be hinted by the slender shoulder peaking to the left-hand side of the dominant FTO substrate peak, which becomes more definite with the increase of the TT temperature. The other anatase maxima (*i.e.*, 004, 112) are overlaid by the higher intensity reflections from the substrate, and thereby, are difficult to discriminate.

The crystalline coherence length ("crystallite size") was calculated from the FWHM of the 101 diffraction line of anatase, using the Scherrer equation [32]. The line width was

corrected for instrumental broadening using a corundum standard reference (NIST-SRM 1976a). As expected, the crystallite size (D_{101}) gradually increased with the post-synthesis heat-treatment temperature from ~19 nm (at 450°C) to ~39 nm (at 630°C) (see Fig. 2-inset).

TiO_2 NTs on Ti substrate were sintered from 450 to 700°C [33]. One observed that the rutile phase appears at 450°C, to become dominant at 600°C. The rutile phase was not observed for the TiO_2 NTs onto FTO glass at 630 °C, probably due to different substrates underneath nanotubes. Feng *et al.* [34] noticed that the rutile phase appears at a lower temperature if TiO_2 NT is on Ti plate. On the other hand, they found out that the freestanding TiO_2 NT membrane (without substrate) retains an anatase phase when increasing the temperature to 800°C. Anatase to rutile transformation is faster in case of TiO_2 NTs onto titanium plate because the rutile phase nucleation and growth occur at the interfaces between nanotubes and titanium substrate. For the freestanding membrane, there is however not enough space for rotation and transformation of anatase crystals to rutile. Ti substrate accordingly speeds up the anatase to rutile transformation, not observed in the case of FTO substrate [35]. The presence of rutile phase in TiO_2 NTs onto FTO glass was therefore not observable.

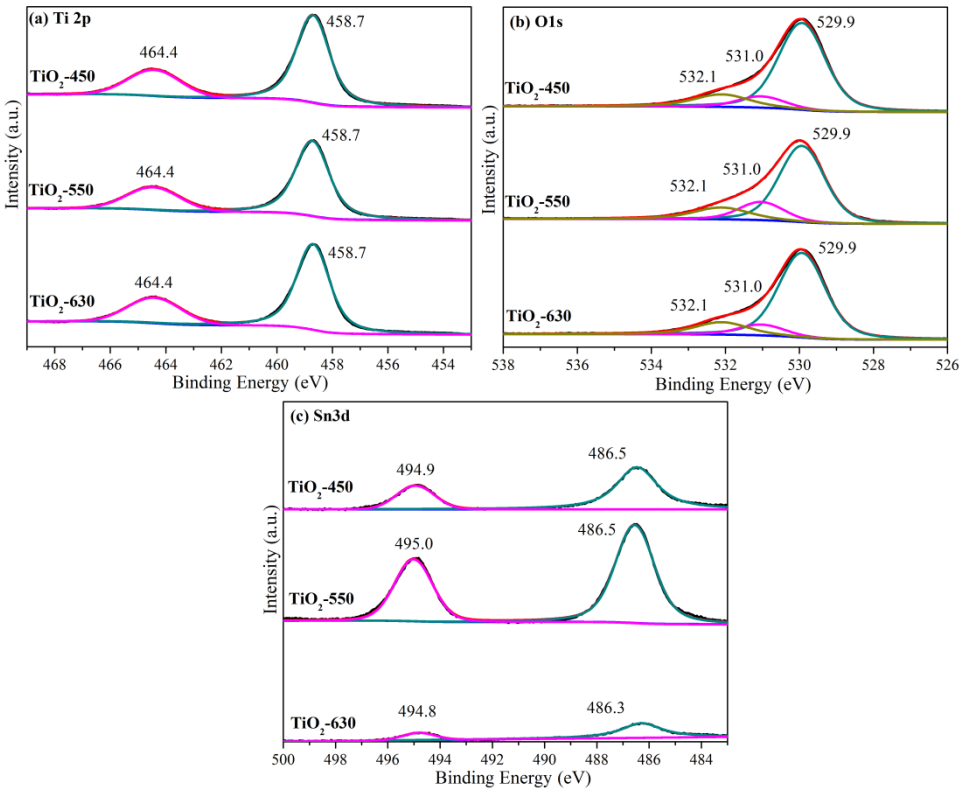

Fig. 3. XPS spectra of Ti 2p (a), O1s (b) and Sn 3d (c) of TiO_2 NT arrays annealed in air at 450, 550 and 630°C (black line - data, red line - fit, blue line - background, dark cyan - peak 1, magenta - peak 2, dark yellow - peak 3).

The XPS measurements were recorded for the sintered TiO_2 films to investigate chemical composition and the oxidation state of elements. Wide scans revealed the presence of C, Ti, O and Sn elements in the NT arrays (data not shown here). All annealed samples exhibit two main Ti 2p peaks located at 458.7 eV (Ti $2p_{3/2}$) and 464.4 eV (Ti $2p_{1/2}$), and the difference between these two components is 5.7 eV, which corresponds to the anatase phase [36]. It is indicative for the presence of Ti^{4+} chemical state in TiO_2 lattice [36]. No shifts were observed, regardless of the annealing temperature (Fig. 3a). Zatsepin *et al.* [37] also noticed

no Ti 2p shift after Sn implantation into TiO_2 thin film. As visible from Fig. 3b, the O 1s peaks feature three main components: (*i*) 529.9 eV corresponding to lattice oxygen bonded to Ti; (*ii*) 531.0 eV, which could be ascribed to hydroxide or oxygen in organic compounds; and (*iii*) 532.1 eV is probably surface H_2O group [29,31]. As it can be seen from Fig. 3c, all annealed samples exhibit Sn, seemingly in lower contents in the case of TiO_2-630. When comparing the position of Sn in FTO, with that in TiO_2 films (Table I), it is evident that the binding energy of Sn decreases with the increase of the annealing temperature. This could be due to changes in electron density, suggesting leaching and diffusion of Sn from underlying FTO layer into TiO_2 NTs thin film. A similar trend was observed for nanotubular hematite photodiodes, which were sintered at 800°C. It was found that a high annealing temperature induced the diffusion of Sn from FTO into hematite. With increasing sintering treatment time, the Sn $3d_{3/2}$ and Sn $3d_{5/2}$ peaks shifted to lower binding energies. Because the electronegativity of Sn (1.96) is superior to that of Fe (1.83), the Sn 3d peaks shifted to lower binding energies when Sn was incorporated into the FeO matrix [18]. XPS analysis revealed the presence of Sn in TiO_2 nanotube arrays, at the concentration level of 0.6 to 3.9 at.%, where the highest amount (3.9 at.%) is for the 550°C heat-treated sample. The Sn was found to drastically decrease when a 630°C annealing was applied.

Tab. I Peaks positions in the case of the Ti 2p, O 1s and Sn 3d core electron levels for the bare FTO glass and TiO_2 NT arrays annealed in air at 450, 550 and 630°C.

Sample type	**Ti $2p_{1/2}$, eV**	**Ti $2p_{3/2}$, eV**	**O 1s, eV**			**Sn $3d_{5/2}$, eV**	**Sn $3d_{3/2}$, eV**
FTO	/	/	530.4	531.7	533.1	486.7	495.2
TiO_2-450	464.4	458.7	529.9	531.0	532.1	486.5	494.9
TiO_2-550	464.4	458.7	529.9	531.0	532.1	486.5	495.0
TiO_2-630	464.4	458.7	529.9	531.0	532.1	486.3	494.8

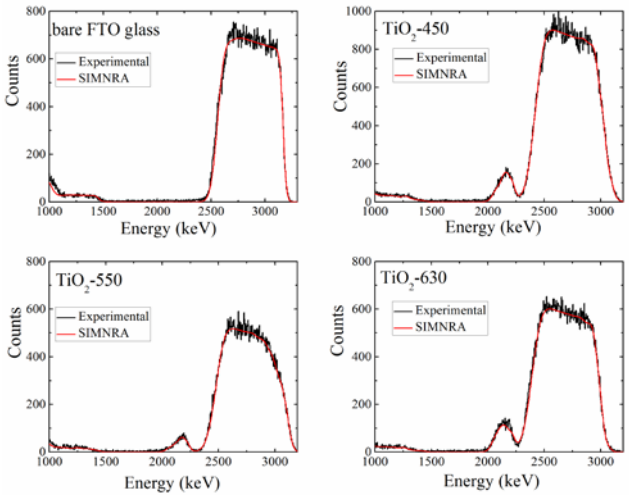

Fig. 4. Experimental and simulated RBS spectra of bare FTO glass and TiO_2 NT films deposited onto FTO glass and annealed in air at 450, 550 and 630°C.

As XPS is basically a surface sensitive method, RBS and ToF-ERDA measurements were further carried out to investigate the diffusion of Sn into the TiO_2 nanotubes depth. From experimental and simulated RBS spectra, shown in Fig. 4, the presence of Sn (observed around 2500-3000 keV) and Si (seen below 1500 keV), can be observed for bare FTO glass. The presence of oxygen could not be detected, since the contribution of light elements is generally small for Li beam RBS, and this part of spectra is cut away. The RBS spectra of the annealed TiO_2-NT samples evidenced the presence of Sn and Si (originating from the FTO glass substrate), but also a new peak, around 2000-2500 keV, that is assigned to Ti in TiO_2 NT film.

The SIMNRA code was used for the simulation of the experimental data, which provides information on the stoichiometry and areal concentration of the samples (Fig. 5) with an uncertainty of the fit estimated to 5 %. The RBS-technique mass resolution for light elements is limited and, as a result, in the aforementioned figures, the depth profiles of C, N, O and F are given as a total sum denoted as "light elements". The thickness of the samples annealed at 450 and 550°C is 1250 × 10^{15} at/cm^2, increases to 1370 × 10^{15} at/cm^2 for 630°C. The TiO_2-630 film is thereby thicker or denser. Sn diffuses into all samples, to reach ~500 × 10^{15} at/cm^2 from the surface of TiO_2 NT films in case of 450 and 550°C annealing. In the case of the 630°C-treated TiO_2 NT films, the diffusion had a shorter path, ending to 975 × 10^{15} at/cm^2 from the surface. It should be emphasized that Fig. 5 shows an average thickness of the TiO_2 film, corresponding to a density of 4.23 g/cm^2 (for pure anatase). On the other hand, TiO_2 film is not homogeneous due to nanotube morphology. It is to note that the additional energy straggling of incoming and recoiled ions produces the broadening of measured energy spectra at the TiO_2–SnO_2 interface. Nevertheless, the simulation of this extra contribution in energy straggling was impossible, even by MC code. Fig. 5 presents therefore the depth profile as a convolution of diffusion between the layers and energy straggling via the non-homogeneous media.

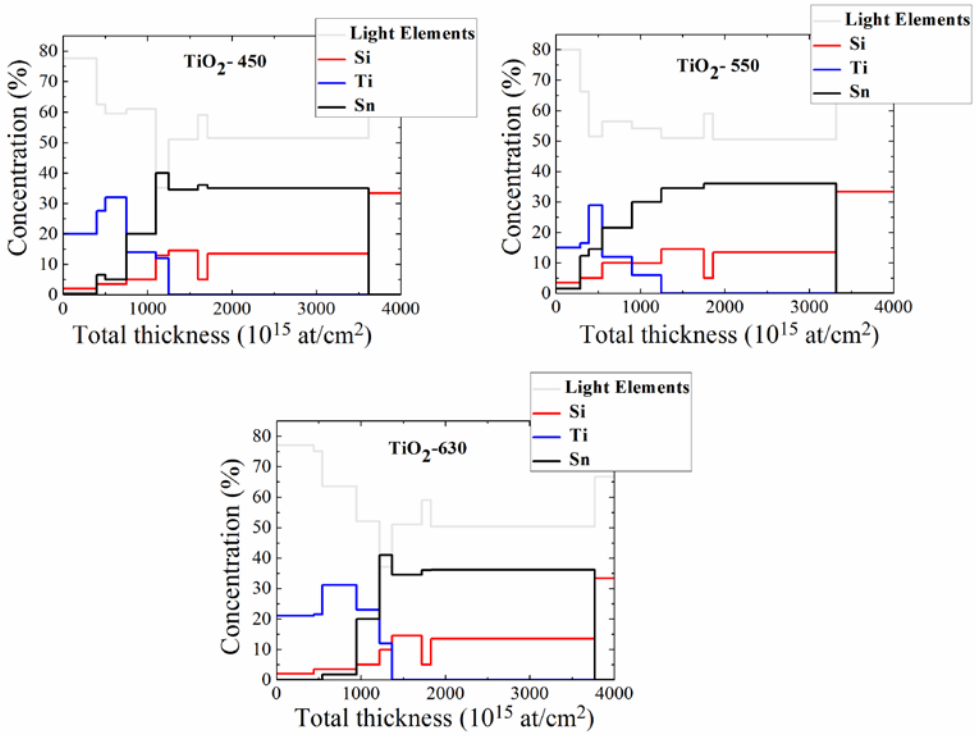

Fig. 5. The depth profiles by RBS measurements in the case of TiO_2 NT samples, annealed in air at 450, 550 and 630°C.

Besides the Sn, a Ti diffusion into SnO_2 film was also evident. The interfaces between the two elements were situated for the 450, 550 and 630°C annealed samples at 500 × 10^{15}, 550 × 10^{15} or 975 × 10^{15} at/cm^2, respectively. According to these results, it follows that Sn diffuses into TiO_2 films in all cases, with a maximum for the TiO_2-550 sample. It is suggested that competition takes place between the diffusion of Sn into TiO_2 and Ti into SnO_2 films. At 450 and 550°C, Sn diffused up to ~500-550 × 10^{15} at/cm^2, while at 630°C, the corresponding diffusion extends to ~950 × 10^{15} at/cm^2.

Additional elemental depth profile investigations were carried out by ToF-ERDA and the results are provided in Fig. 6. Herein, it is also evident that TiO_2 film is denser at 630°C, and it seems that Sn diffusion is lower than for 450 and 550°C. It can be seen that when increasing atomic content of Sn, Ti content starts to decrease, pointing to the existence of an interface between the TiO_2 and SnO_2 layers, with a mix of TiO_2 and SnO_2 (interface). The estimated thickness of TiO_2 layers by ToF-ERDA is smaller than measured by RBS (Fig. 5).

On the other hand, as visible from Fig. 1, after the annealing, the surface morphology of TiO_2 layer is not flat, but porous due to formation of NT arrays. Also, since the beam in ToF-ERDA has been oriented 20° against the sample surface, the average thickness of measured films is actually lower than obtained by RBS, where the beam incidence angle was 90° with respect to the sample surface. ToF-ERDA results must be therefore considered from a qualitative point of view only.

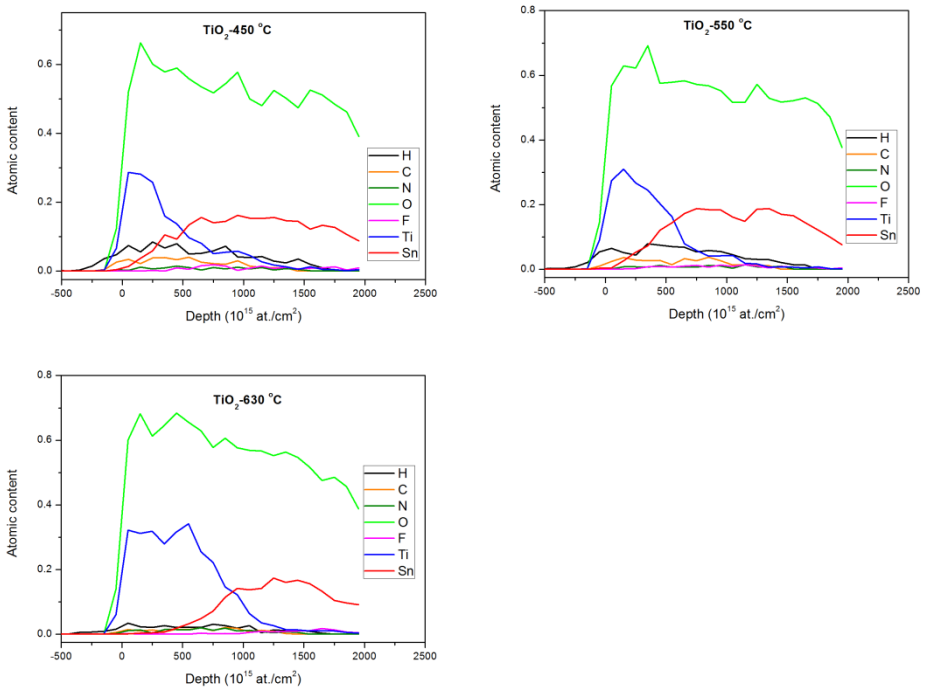

Fig. 6. ToF-ERDA depth profile measurements of the TiO_2 NT arrays samples annealed in air at 450, 550 and 630°C.

The interpretation of the optical properties of the annealed TiO_2 NT samples is introduced with Fig. 7. The absorption edges were inferred from the maxima of the DRS, as proposed by Murphy [39]. The annealing temperature has not significantly affected the absorption edge of the films, but a slight red shift of wavelength was still observed. Actually, the sample with higher diffusion of Sn (i.e., TiO_2-550) had the highest absorption shift, while TiO_2-630 had the smallest one, along with a lower amount of diffused Sn.

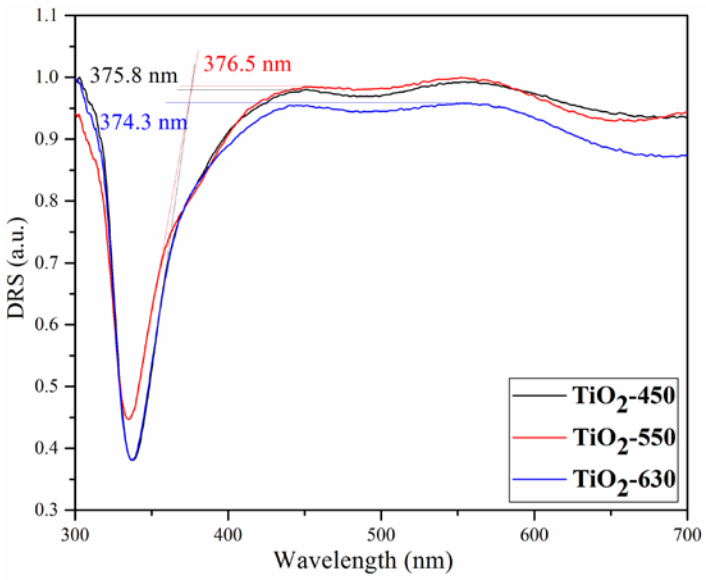

Fig. 7. DRS spectra of the TiO_2-450, TiO_2-550 and TiO_2-630 samples, respectively.

According to the results from RBS and ToF-ERDA analysis, it can be seen that the TiO_2 film is thicker (or denser) for the sample sintered at 630°C compared to the sintering at 450 and 550°C. The XRD analysis showed better crystalline quality for higher temperatures of sintering. Having all this in mind, the lower content of Sn in TiO_2-630 is probably due to changes in crystallinity, thickness, and morphology of the TiO_2. Bjelajac et al. [23] sintered TiO_2 NTs onto FTO at 500°C and observed diffusion of 0.15 at.% Sn into TiO_2. They sintered for 2 h, while in this study annealing was done for a half hour and observed higher Sn content. The reason for that could be different speed heating and time of annealing. Further research efforts should focus on optimizing the temperature of annealing with other parameters of annealing such as speed heating and time of annealing. Besides this, the DRS results showed a trend in a red shift as the amount of Sn in TiO_2 NTs increases, which can improve the photoactivity of TiO_2. This diffusion of Sn in TiO_2 during thermal treatment can be beneficial as can be seen from the literature. For example, according to the Ref. [20], the photoactivity is enhanced in the case of hematite photoanodes due to Sn diffusion from FTO glass into hematite. This shows that the annealing temperature influences the formation of the TiO_2-SnO_2 interface that plays an important role in the photoactivity of TiO_2. Perovskite solar cells with TiO_2/SnO_2 bilayer demonstrated higher efficiency than solar cells with solely TiO_2 or SnO_2 layer. This is because bilayer enables a higher electron extraction driving force and a stronger hole blocking ability due to the defect-free physical contact at the interface [40]. Our study reports on the detailed chemical analysis of the TiO_2/SnO_2 mix phase obtained by annealing of anodized TiO_2 NTs on FTO. The results support the continuation of this investigation line to gain better photo performances of TiO_2 NTs/FTO based structures.

4. Conclusion

TiO_2 nanotube arrays were synthesized perpendicularly to the FTO support via an anodization method in ethylene glycol electrolyte. The as-obtained amorphous TiO_2 nanotube arrays were annealed at three different temperatures (450, 550 and 630°C) to study the possible chemical and morphological changes. According to GIXRD investigations, the samples consisted of an anatase sole phase, whose crystalline status of the TiO_2 nanotubes array increased with thermal-treatment temperature. The mean crystallite size grew

progressively from ~19 nm (at 450°C) to ~39 nm (at 630°C). The sintering temperature influenced the Sn diffusion into TiO_2 NT, where the highest concentration of Sn was reached for the 550°C heat-treated sample. The amount of Sn drastically decreased when a 630°C annealing was applied. The chemical distributions of elements, along with the nanotubes depth were studied by RBS and ToF-ERDA. Sn diffusion was less extensive for 630°C-annealed samples, in comparison with those heat-treated at 450 and 550°C. Besides Sn diffusion, the Ti into SnO_2 film was also observed. With the increase of atomic content of Sn, Ti content started to decrease, pointing to the existence of an interface between the TiO_2 and SnO_2 layers, where the presence is assumed of a mixed phase of TiO_2 and SnO_2. The observed evolutions are expected to strongly influence the convertibility of TiO_2 anatase layers of UV to Vis absorption for a new generation of electrical energy sources under solar illumination. The developed structures can be further used for electrodes preparation for more efficient solar cells.

Acknowledgments

This work was supported by the Ministry of Education, Science and Technological Development of the Republic of Serbia (Contract No. 451-03-9/2021-14/200175 for ITN SASA, 451-03-9/2021-14/200135 for TMF). XPS and ToF-ERDA/RBS analyses were accomplished thanks to the financial support of the CERIC-ERIC (20177018 proposal) and Structure Fund Project CZ.02.1.01/0.0/0.0/16_013/0001788. GES thanks to Core Programme 21N and to CNCS/CCCDI – UEFISCDI, project number PN-III-P1-1.1-TE-2019-0688, within PNCDI III. G.S. and I.N.M. acknowledge the support by a grant of the CCCDI - UEFISCDI, project number PN-III-P2-2.1-PED-2019-4642, within PNCDI III.

5. References

1. M. A. Green, P. A. Basore, N. Chang, D. Clugston, R. Egan, R. Evans, D. Hogg, S. Jarnason, M. Keevers, P. Lasswell, J. O'Sullivan, U. Schubert, A. Turner, S. R. Wenham, T. Young, Crystalline silicon on glass (CSG) thin-film solar cell modules, Sol. Energy, 77 (2004) 857-863.
2. W. Cai, X. Gong, Y. Cao, Polymer solar cells: Recent development and possible routes for improvement in the performance, Sol. Energy Mater. Sol. Cells. 94 (2010) 114-127.
3. A. H. Ip, S. M. Thon, S. Hoogland, O. Voznyy, D. Zhitomirsky, R. Debnath, L. Levina, L. R. Rollny, G. H. Carey, A. Fischer, K. W. Kemp, I. J. Kramer, Z. Ning, A. J. Labelle, K. W. Chou, A. Amassian, E.H. Sargent, Hybrid passivated colloidal quantum dot solids, Nat. Nanotechnol, 7 (2012) 577-582.
4. A. Bjelajac, V. Djokic, R. Petrovic, G.E. Stan, G. Socol, I. N. Mihailescu, D. Janackovic, R. Physics, Pulsed laser deposition method for fabrication of CdS/TiO_2 and PbS photoelectrodes for solar energy application, Dig. J. Nanomater. Biostructures, 10 (2015) 1411-1418.
5. B. E. Hardin, H. J. Snaith, M. D. McGehee, The renaissance of dye-sensitized solar cells, Nat. Photonics, 6 (2012) 162-169.
6. R. Salazar, M. Altomare, K. Lee, J. Tripathy, R. Kirchgeorg, N. T. Nguyen, M. Mokhtar, A. Alshehri, S. A. Al-Thabaiti, P. Schmuki, Use of Anodic TiO_2 Nanotube Layers as Mesoporous Scaffolds for Fabricating CH3NH3PbI3 Perovskite-Based Solid-State Solar Cells, ChemElectroChem., 2 (2015) 824-828.
7. H. Y. Yang, W. Y. Rho, S. K. Lee, S. H. Kim, Y. B. Hahn, TiO_2 nanoparticles/nanotubes for efficient light harvesting in perovskite solar cells,

Nanomaterials, 9 (3) (2019) 326.
8. J. Bai, B. Zhou, Titanium dioxide nanomaterials for sensor applications, Chem. Rev., 114 (2014) 10131-10176.
9. Y. Liu, Y. Yang, Recent Progress of TiO_2 -Based Anodes for Li Ion Batteries, J. Nanomater., 2016 (2016) 1-15.
10. F. Parast, M. Montazeri-Pour, M. Rajabi, F. Bavarsiha, Comparison of the structural and photo-catalytic properties of nanostructured Fe_3O_4/TiO_2 core-shell composites synthesized by ultrasonic and stöber methods, Sci. Sinter., 52 (2020) 415-432.
11. M. R. Gauna, J. M. Martinez, M. S. Conconi, G. Suárez, N. M. Rendtorff, Effect of TiO_2 in fine zircon sintering and properties, Sci. Sinter., 53 (2021) 267-283.
12. Y. L. Pang, S. Lim, H. C. Ong, W. T. Chong, A critical review on the recent progress of synthesizing techniques and fabrication of TiO_2-based nanotubes photocatalysts, Appl. Catal. A Gen., 481 (2014) 127-142.
13. P. Roy, D. Kim, K. Lee, E. Spiecker, P. Schmuki, TiO_2 nanotubes and their application in dye-sensitized solar cells., Nanoscale., 2 (2010) 45-59.
14. T. Kasuga, M. Hiramatsu, A. Hoson, T. Sekino, K. Niihara, Formation of Titanium Oxide Nanotube, Langmuir., 14 (1998) 3160-3163.
15. T. Maiyalagan, B. Viswanathan, U. V. Varadaraju, Fabrication and characterization of uniform TiO_2 nanotube arrays by sol-gel template method, Bull. Mater., 29 (2006) 705-708.
16. M. Krbal, H. Sopha, V. Podzemna, S. Das, J. Prikryl, J. M. Macak, TiO_2 Nanotube/Chalcogenide-Based Photoelectrochemical Cell: Nanotube Diameter Dependence Study, J. Phys. Chem. C., 121 (2017) 6065-6071.
17. G. Li, Z.-Q. Liu, J. Lu, L. Wang, Z. Zhang, Effect of calcination temperature on the morphology and surface properties of TiO2 nanotube arrays, Appl. Surf. Sci. 255 (2009) 7323-7328.
18. A. Annamalai, A. Subramanian, U. Kang, H. Park, S. H. Choi, J. S. Jang, Activation of Hematite Photoanodes for Solar Water Splitting: Effect of FTO Deformation, J. Phys. Chem. C., 119 (2015) 3810-3817.
19. C. Hudaya, J. Park, J. Lee, Effects of process parameters on sheet resistance uniformity of fluorine-doped tin oxide thin films, Nanoscale Res. Lett., 7 (2012) 17.
20. P. S. Shinde, A. Annamalai, J. H. Kim, S. H. Choi, J. S. Lee, J. S. Jang, Exploiting the dynamic Sn diffusion from deformation of FTO to boost the photocurrent performance of hematite photoanodes, Sol. Energy Mater. Sol. Cells., 141 (2015) 71-79.
21. C. Andrei, T. O'Reilly, D. Zerulla, A spatially resolved study on the Sn diffusion during the sintering process in the active layer of dye sensitised solar cells, Phys. Chem. Chem. Phys., 12 (2010) 7241-7245.
22. J. Shang, W. Yao, Y. Zhu, N. Wu, Structure and photocatalytic performances of glass/SnO_2/TiO_2 interface composite film, Appl. Catal. A Gen. 257 (2004) 25-32.
23. A. Bjelajac, R. Petrović, J. Vujancevic, K. Veltruska, V. Matolin, Z. Siketic, G. Provatas, M. Jaksic, G.E. Stan, G. Socol, I.N. Mihailescu, D. Janaćković, Sn-doped TiO_2 nanotubular thin film for photocatalytic degradation of methyl orange dye, J. Phys. Chem. Solids., 147 (2020) 1-8.
24. Y. Li, Q. Zhang, L. Niu, J. Liu, X. Zhou, TiO_2 nanorod arrays modified with SnO_2-Sb_2O_3 nanoparticles and application in perovskite solar cell, Thin Solid Films. 621 (2017) 6-11.
25. C. S. Chua, O. K. Tan, M. S. Tse, X. Ding, Photocatalytic activity of tin-doped TiO_2 film deposited via aerosol assisted chemical vapor deposition, Thin Solid Films. 544 (2013) 571-575.
26. K. Shankar, G. K. Mor, H. E. Prakasam, S. Yoriya, M. Paulose, O. K. Varghese, C. A. Grimes, Highly-ordered TiO_2 nanotube arrays up to 220 μm in length: Use in

water photoelectrolysis and dye-sensitized solar cells, Nanotechnology, 18 (2007) 065707.
27. H. Zheng, A.Z. Sadek, M. Breedon, D. Yao, K. Latham, J. du Plessis, K. Kalantar-Zadeh, Fast formation of thick and transparent titania nanotubular films from sputtered Ti, Electrochem. Commun., 11 (2009) 1308-1311.
28. M. Mayer, SIMNRA, a simulation program for the analysis of NRA, RBS and ERDA, in: AIP Conf. Proc., AIP, 1999: pp. 541-544.
29. Z. Siketić, I.B. Radović, M. Jakšić, Development of a time-of-flight spectrometer at the Ruder Bošković Institute in Zagreb, Nucl. Instruments Methods Phys. Res. Sect. B Beam Interact. with Mater. Atoms., 266 (2008) 1328-1332.
30. Z. Siketić, I. B. Radović, M. Jakšić, Quantitative analysis of hydrogen in thin films using Time-of-Flight Elastic Recoil Detection Analysis, Thin Solid Films, 518 (2010) 2617-2622.
31. K. Arstila, J. Julin, M.I. Laitinen, J. Aalto, T. Konu, S. Kärkkäinen, S. Rahkonen, M. Raunio, J. Itkonen, J. P. Santanen, T. Tuovinen, T. Sajavaara, Potku - New analysis software for heavy ion elastic recoil detection analysis, Nucl. Instruments Methods Phys. Res. Sect. B Beam Interact. with Mater. Atoms. 331 (2014) 34-41.
32. L. Patterson, The scherrer formula for X-ray particle size determination, Phys. Rev. 56 (1939) 978-982.
33. J. Vujančević, A. Bjelajac, J. Ćirković, V. Pavlović, E. Horvath, L. Forró, B. Vlahović, M. Mitrić, Đ. Janaćković, V. Pavlović, Structure and photocatalytic properties of sintered TiO_2 nanotube arrays, Sci. Sinter., 50 (2018) 39-50.
34. D. Fang, Z. Luo, K. Huang, D. C. Lagoudas, Effect of heat treatment on morphology, crystalline structure and photocatalysis properties of TiO_2 nanotubes on Ti substrate and freestanding membrane, Appl. Surf. Sci., 257 (2011) 6451-6461.
35. R. Taziwa, E. Meyer, S. Zinya, A microscopy study of the effect of annealing temperature on the morphological and structural properties of titanium dioxide nanotubes fabricated on functional substrates, Int. J. Nanotechnol. Med. Eng., 3 (2018) 16-27.
36. M. C. Biesinger, L. W. M. Lau, A. R. Gerson, R. S. C. Smart, Resolving surface chemical states in XPS analysis of first row transition metals, oxides and hydroxides: Sc, Ti, V, Cu and Zn, Appl. Surf. Sci., 257 (2010) 887-898.
37. D. A. Zatsepin, D. W. Boukhvalov, E. Z. Kurmaev, I. S. Zhidkov, S. S. Kim, L. Cui, N. V. Gavrilov, S. O. Cholakh, XPS and DFT study of Sn incorporation into ZnO and TiO_2 host matrices by pulsed ion implantation, Phys. Status Solidi Basic Res., 252 (2015) 1890-1896.
38. G. Ayyakannu Sundaram, M. Yang, K. Nomura, S. Maniarasu, G. Veerappan, T. Liu, J. Wang, ^{119}Sn Mössbauer and Ferromagnetic Studies on Hierarchical Tin- and Nitrogen-Codoped TiO_2 Microspheres with Efficient Photocatalytic Performance, J. Phys. Chem. C., 121 (2017) 6662-6673.
39. A. B. Murphy, Band-gap determination from diffuse reflectance measurements of semiconductor films, and application to photoelectrochemical water-splitting, Sol. Energy Mater. Sol. Cells., 91 (2007) 1326-1337.
40. H. Xie, X. Yin, J. Liu, Y. Guo, P. Chen, W. Que, G. Wang, B. Gao, Low temperature solution-derived TiO_2-SnO_2 bilayered electron transport layer for high performance perovskite solar cells, Appl. Surf. Sci. 464 (2019) 700-707.

Сажетак: *Чисти Ti филмови депоновани су радио-фреквентним магнетним спатеровањем на ФТО стаклу да би се синтетисали филмови TiO_2 наноцеви (НЦ). TiO_2 НЦ/ФТО узорци су синтеровани на 450, 550 и 630°C, у ваздуху. Термички третман није утицао на састав кристалне фазе, сачувајући у свим узорцима само једну фазу,*

анатас. Као што се очекивало, кристалиничност анатаса се побољшала са температуром жарења. Ипак, мале разлике у морфологији наноцеви, као што је изглед зрна унутар зидова, примећене су у случају узорка синтерованог на 630°C. Применом фотоелектронске спектроскопије X-зрака урађена је хемијска анализа жарених узорака при чему је утврђено присуство Sn унутар TiO_2 наноцеви, услед дифузије Sn из супстрата у TiO_2. За супстрат је коришћено ФТО стакло чији се горњи слој састоји од SnO_2 допиран са F. RBS спектроскопија и спектроскопија еластично избијених јона мерењем времена пролета су спроведена ради проучавања профила дубине филмова. Утврђено је да температура синтеровања контролише дифузију Sn унутар филма TiO_2. Атоми Sn дифундују према површини TiO_2 НЦ за узорке жарене на 450 и 550°C. Дифузија је међутим отежана у случају термичког третмана на 630°C. Осим тога, примећена је дифузија Ti у SnO_2 слоју, при чему се формирао међуслој TiO_2/SnO_2. Није уочена велика разлика у апсорпцији између узорака, пошто сви узорци садрже анатас фазу, што је потврђено спектроскопијом дифузионе рефлексије. Међутим, уочена је већа количина Sn код узорка жареног на 550°C, што је довело до благог црвеног апсорпционог помераја. Важност контроле параметара жарења анодизованих TiO_2/ФТО структура је наглашена кроз формирање TiO_2-SnO_2 међуслоја и дифузије Sn из ФТО, што може играти суштинску улогу у повећању фотоперформанси фотонапонских структура заснованих на TiO_2 НЦ/ФТО.

***Кључне речи**: Sn дифузија, Sn-TiO_2 допирање, синтеровање, ToF-ERDA, XPS.*